Crystal structure of ponazuril, $C_{18}H_{14}F_3N_3O_6S$

James A. Kaduk,[1,2,a] Stacy Gates-Rector,[3] and Thomas N. Blanton[3]
[1]*Illinois Institute of Technology, 3101 S. Dearborn St., Chicago, IL 60616, USA*
[2]*North Central College, 131 S. Loomis St., Naperville, IL 60540, USA*
[3]*ICDD, 12 Campus Blvd., Newtown Square, PA 19073-3273, USA*

(Received 28 June 2022; accepted 12 September 2022)

The crystal structure of ponazuril has been solved and refined using synchrotron X-ray powder diffraction data, and optimized using density functional theory techniques. Ponazuril crystallizes in space group $P2_1/c$ (#14) with $a = 8.49511(6)$, $b = 12.38696(6)$, $c = 18.84239(17)$ Å, $\beta = 96.7166(4)°$, $V = 1969.152(12)$ Å^3, and $Z = 4$. N–H···O hydrogen bonds link the molecules into chains along the *a*-axis, with a graph set *C1,1(6)*. The powder pattern has been submitted to ICDD for inclusion in the Powder Diffraction File™ (PDF®). [doi:10.1017/S0885715622000409]

Key words: ponazuril, Marquis®, Toltrazuril sulfone®, Ponalrestat®, powder diffraction, Rietveld refinement, density functional theory

I. INTRODUCTION

Ponazuril (sold under the brand names Toltrazuril sulfone®, Marquis®, and Ponalrestat®) is an antiprotozoal medication used to treat equine protozoal myeloencephalitis (EPM). While it is labeled for use in horses, it is also used in cats, dogs, rabbits, birds, and reptiles to treat coccidiosis due to protozoal parasites. The systematic name (CAS Registry No. 69004-04-2) is 1-methyl-3-[3-methyl-4-[4-(trifluoromethylsulfonyl)phenoxy]phenyl]-1,3,5-triazinane-2,4,6-trione. A two-dimensional molecular diagram is shown in Figure 1.

A powder pattern of crystalline ponazuril has been reported by Li *et al.* (2022), in the context of a study of preparation of co-amorphous formulations of toltrazuril and ponazuril, but no crystal structure of ponazuril was reported.

This work was carried out as part of a project (Kaduk *et al.*, 2014) to determine the crystal structures of large-volume commercial pharmaceuticals, and include high-quality powder diffraction data for them in the Powder Diffraction File (Gates-Rector and Blanton, 2019).

II. EXPERIMENTAL

Ponazuril was a commercial reagent, purchased from TargetMol (Lot #131432), and was used as-received. The white powder was packed into a 1.5 mm diameter Kapton capillary and rotated during the measurement at ~50 Hz. The powder pattern was measured at 295 K at beamline 11-BM (Antao *et al.*, 2008; Lee *et al.*, 2008; Wang *et al.*, 2008) of the Advanced Photon Source at Argonne National Laboratory using a wavelength of 0.458208(2) Å from 0.5 to 50° 2θ with a step size of 0.0009984375 and a counting time of 0.1 s per step. The high-resolution powder diffraction data were collected using twelve silicon crystal analyzers that allow for high angular resolution, high precision, and accurate peak positions. A mixture of silicon (NIST SRM 640c) and

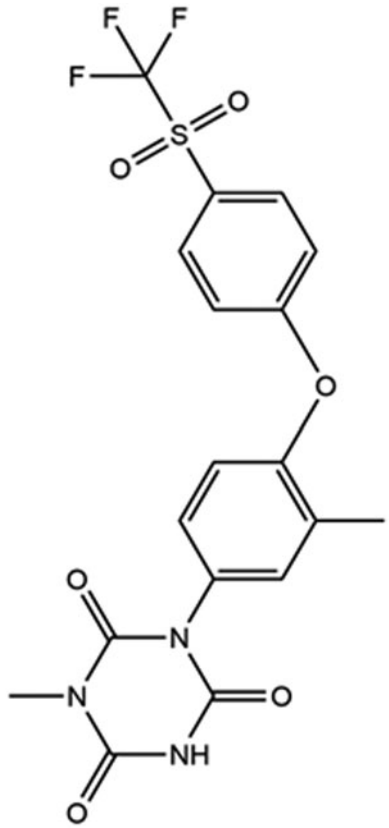

Figure 1. The 2D molecular structure of ponazuril.

[a]Author to whom correspondence should be addressed. Electronic mail: kaduk@polycrystallography.com

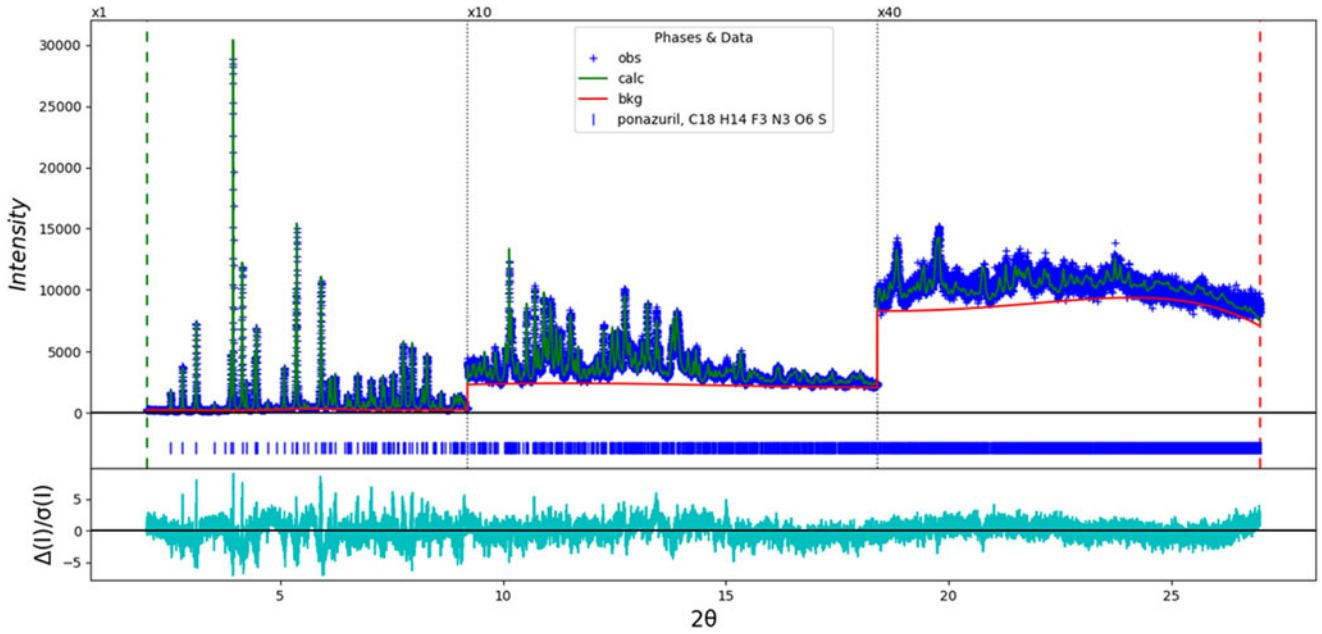

Figure 2. The Rietveld plot for the refinement of ponazuril. The blue crosses represent the observed data points, and the green line is the calculated pattern. The cyan curve is the normalized error plot. The vertical scale has been multiplied by a factor of 10× for $2\theta > 9.2°$, and by a factor of 40× for $2\theta > 18.4°$. The row of blue tick marks indicates the calculated reflection positions.

alumina (SRM 676a) standards (ratio Al_2O_3:Si = 2:1 by weight) was used to calibrate the instrument and refine the monochromatic wavelength used in the experiment.

The pattern was indexed using JADE Pro (MDI, 2022) and N-TREOR (Altomare *et al.*, 2013) on a primitive monoclinic cell with $a = 8.50462$, $b = 12.39817$, $c = 18.85480$ Å, $\beta = 96.72°$, $V = 1974.41$ Å^3, and $Z = 4$. A reduced cell search in the Cambridge Structural Database (Groom *et al.*, 2016) yielded 16 hits, but no structures of ponazuril derivatives. The suggested space group was $P2_1/c$, which was confirmed by successful solution and refinement of the structure. A diclazuril molecule was downloaded from PubChem (Kim *et al.*, 2019) as Conformer3D_CID_3050408.sdf. It was converted to a *.mol2 file using Mercury (Macrae *et al.*, 2020). The structure was solved by Monte Carlo simulated annealing as implemented in EXPO2014 (Altomare *et al.*, 2013).

Rietveld refinement was carried out using GSAS-II (Toby and Von Dreele, 2013). Only the 2.0–27.0° portion of the

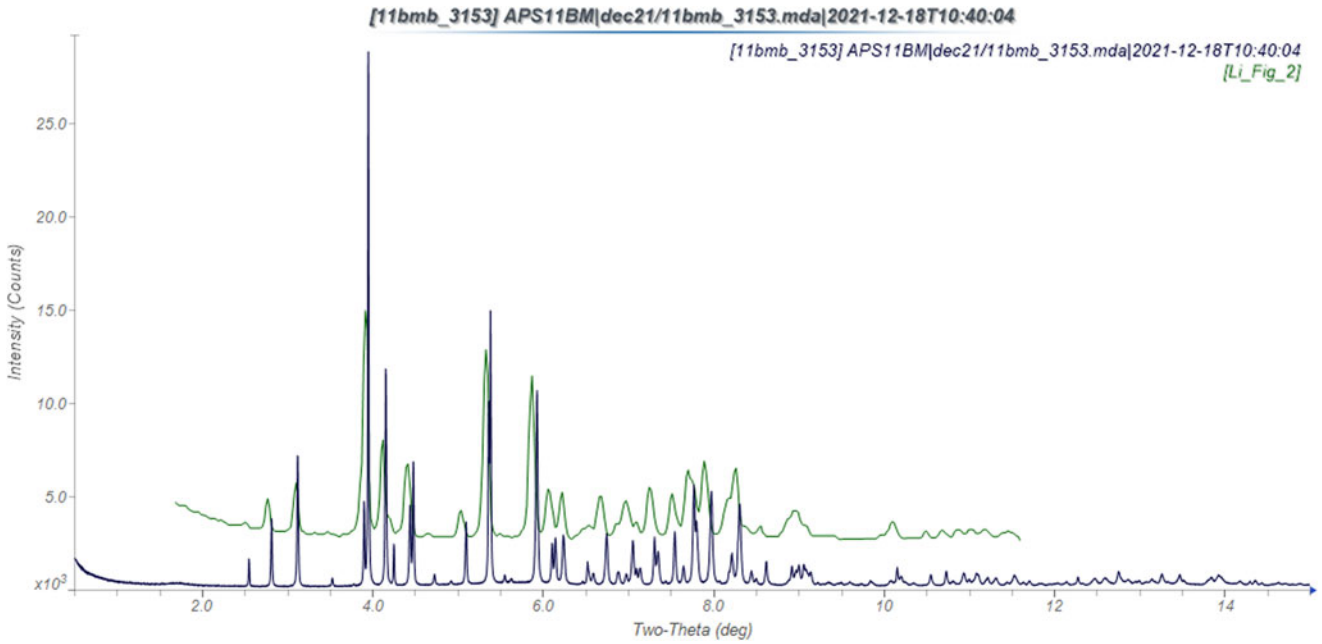

Figure 3. Comparison of the synchrotron pattern from this study of ponazuril (black) to that reported by Li *et al.* (2022; green). The literature pattern, measured using Cu Kα radiation, was digitized using UN-SCAN-IT (Silk Scientific, 2013), and converted to the synchrotron wavelength of 0.458208 Å using JADE Pro (MDI, 2022). Image generated using JADE Pro (MDI, 2022).

https://doi.org/10.1017/S0885715622000409 Published online by Cambridge University Press

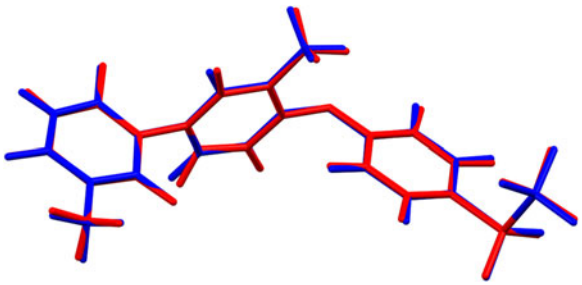

Figure 4. Comparison of the Rietveld-refined (red) and VASP-optimized (blue) structures of ponazuril. The rms Cartesian displacement is 0.066 Å. Image generated using Mercury (Macrae *et al.*, 2020).

pattern was included in the refinement (d_{min} = 0.981 Å). All non-H bond distances and angles were subjected to restraints, based on a Mercury/Mogul Geometry Check (Bruno *et al.*, 2004; Sykes *et al.*, 2011). The Mogul average and standard deviation for each quantity were used as the restraint parameters. The restraints contributed 4.0% to the final χ^2. The hydrogen atoms were included in calculated positions, which were recalculated during the refinement using Materials Studio (Dassault, 2021). The U_{iso} of the heavy atoms were grouped by chemical similarity. The U_{iso} for the H atoms were fixed at 1.2× the U_{iso} of the heavy atoms to which they are attached. A second-order spherical harmonic preferred orientation model was included in the refinement. The refined texture index was 1.007(0). The peak profiles were described using the generalized microstrain model. The background was modeled using a 6-term shifted Chebyshev polynomial, and a peak at 5.72° 2θ to model the scattering from the Kapton capillary and any amorphous component.

The final refinement of 121 variables using 25 040 observations and 84 restraints yielded the residuals R_{wp} = 0.0662 and GOF = 1.49. The largest peak (1.11 Å from F4) and hole (1.14 Å from O8) in the difference Fourier map were 0.32(8) and −0.32(8) eÅ^{-3}, respectively. The largest errors in the difference plot (Figure 2) are in the shapes of some of the strong low-angle peaks.

The crystal structure was optimized using density functional techniques as implemented in VASP (Kresse and Furthmüller, 1996) (fixed experimental unit cell) through the MedeA graphical interface (Materials Design, 2016). The calculation was carried out on 16 2.4 GHz processors (each with 4 GB RAM) of a 64-processor HP Proliant DL580 Generation 7 Linux cluster at North Central College. The calculation used the GGA-PBE functional, a plane wave cutoff energy of 400.0 eV, and a k-point spacing of 0.5 Å^{-1} leading to a 2 × 2 × 1 mesh, and took ∼28.5 h. A single-point density functional calculation (fixed experimental cell) and population analysis were carried out using CRYSTAL17 (Dovesi *et al.*, 2018). The basis sets for the H, C, N, and O atoms in the calculation were those of Gatti *et al.* (1994), and those for F and Cl were those of Peintinger *et al.* (2013). The calculations were run on a 3.5 GHz PC using 8 k-points and the B3LYP functional, and took ∼2.8 h.

III. RESULTS AND DISCUSSION

The synchrotron powder pattern of this study matches the pattern measured by Li *et al.* (2022) well enough to conclude that they represent the same material, and that our sample is representative (Figure 3). The root-mean-square (rms) Cartesian displacement between the Rietveld-refined and DFT-optimized structures of ponazuril is 0.066 Å (Figure 4). The excellent agreement provides strong evidence that the refined structure is correct (van de Streek and Neumann, 2014). This discussion concentrates on the DFT-optimized structure. The asymmetric unit (with atom numbering) is illustrated in Figure 5. The best view of the crystal structure is

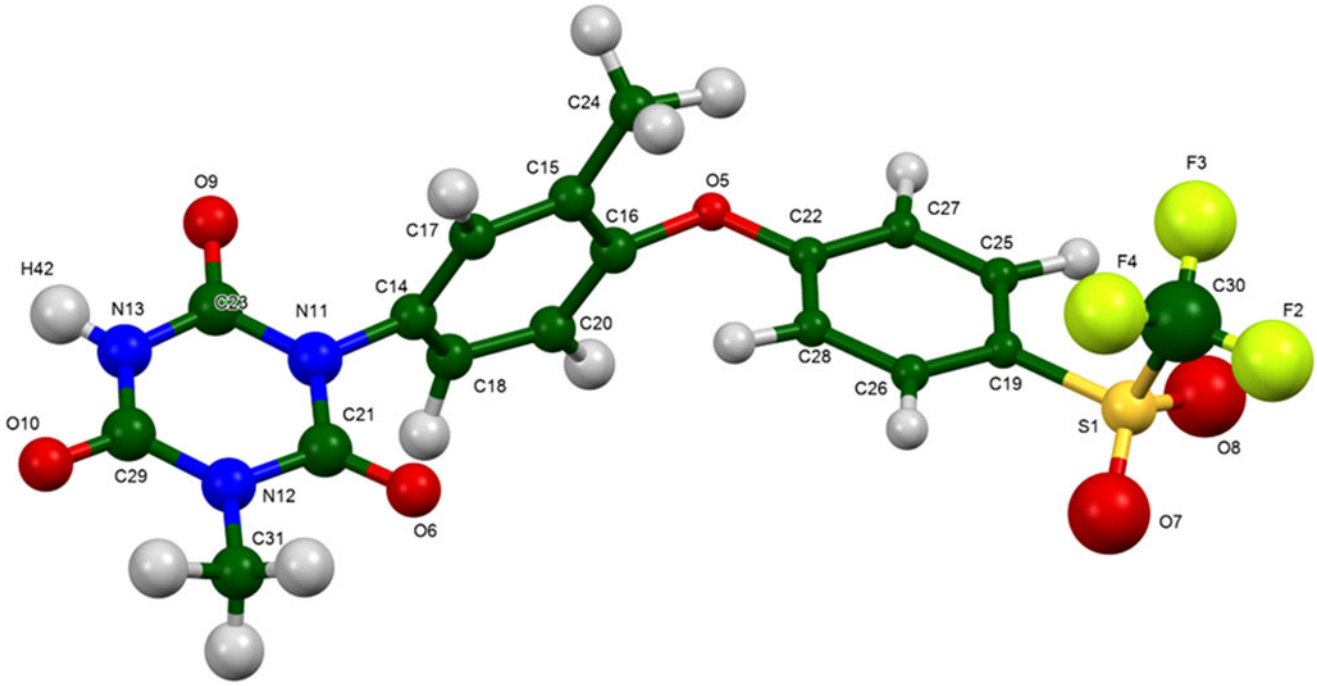

Figure 5. The asymmetric unit of ponazuril, with the atom numbering. The atoms are represented by 50% probability spheroids. Image generated using Mercury (Macrae *et al.*, 2020).

https://doi.org/10.1017/S0885715622000409 Published online by Cambridge University Press

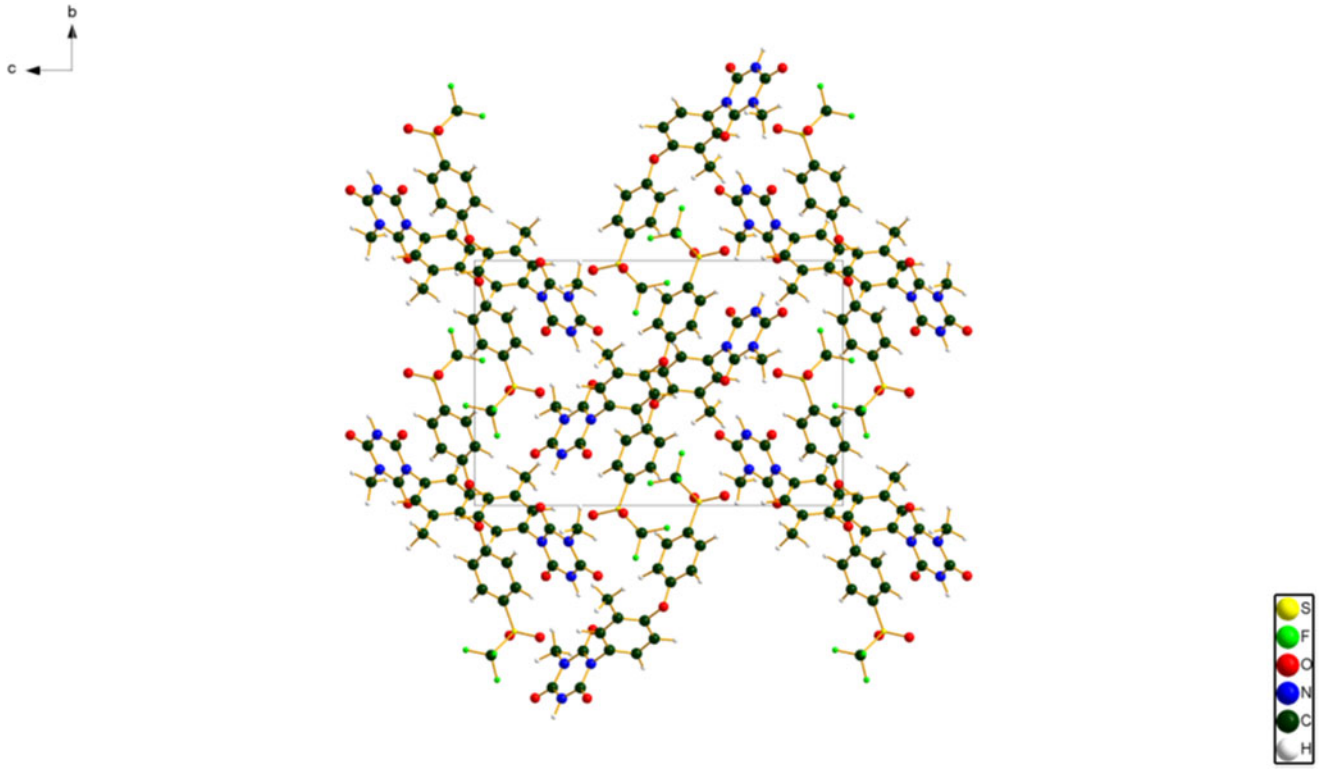

Figure 6. The crystal structure of ponazuril, viewed down the *a*-axis. Image generated using Diamond (Crystal Impact, 2022).

down the *a*-axis (Figure 6). The crystal structure consists of normally packed molecules with hydrogen bonds parallel to the *a*-axis.

All of the bond distances, bond angles, and torsion angles fall within the normal ranges indicated by a Mercury/Mogul Geometry Check (Macrae *et al.*, 2020). Quantum chemical geometry optimization of the ponazuril molecule (DFT/B3LYP/6-31G*/water) using Spartan '18 (Wavefunction, 2020) indicated that the observed conformation is in a local minimum. A conformational analysis (MMFF force field) indicates that the minimum-energy conformation is only 0.1 kcal mol^{-1} lower in energy, but has a very different conformation (Figure 7). The molecule is thus apparently flexible, and intermolecular interactions are important in determining the solid-state conformation.

Analysis of the contributions to the total crystal energy of the structure using the Forcite module of Materials Studio (Dassault, 2021) suggests that the intramolecular deformation energy is dominated by angle and torsion distortion terms. The intermolecular energy is dominated by electrostatic attractions, which in this force field analysis include hydrogen bonds. The hydrogen bonds are better analyzed using the results of the DFT calculation.

There is only one classical hydrogen bond in the structure, N13–H42···O6 (Table I). This interaction between NH and carbonyl groups results in chains along the *a*-axis, with a graph set *C1,1(6)* (Etter, 1990; Bernstein *et al.*, 1995; Shields *et al.*, 2000). By the correlation of Wheatley and Kaduk (2019), this hydrogen bond has an energy of 5.2 kcal mol^{-1}. Several C–H···O hydrogen bonds also contribute to the lattice energy.

The volume enclosed by the Hirshfeld surface of ponazuril (Figure 8, Hirshfeld, 1977; Turner *et al.*, 2017) is 484.29 Å^3, 98.37% of 1/4 the unit cell volume. The packing density is thus fairly typical. The only significant-close contacts (red in Figure 8) involve the hydrogen bonds, and a short C–H···ring distance. The volume/non-hydrogen atom is smaller than usual at 15.9 Å^3.

The Bravais–Friedel–Donnay–Harker (Bravais, 1866; Friedel, 1907; Donnay and Harker, 1937) morphology suggests that we might expect blocky morphology for ponazuril. A second-order spherical harmonic preferred orientation

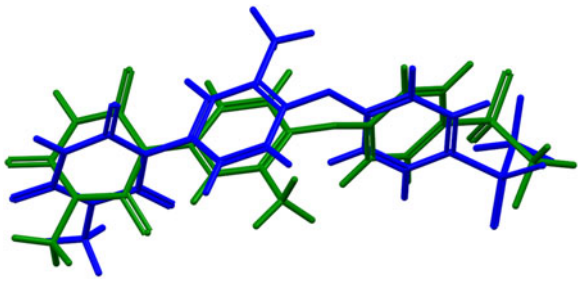

Figure 7. Comparison of the observed solid-state conformation of ponazuril (blue) to the minimum-energy conformation of an isolated molecule (green). Image generated using Mercury (Macrae *et al.*, 2020).

TABLE I. Hydrogen bonds (CRYSTAL17) in ponazuril

H-Bond	D-H (Å)	H···A (Å)	D···A (Å)	D-H···A (°)	Overlap (*e*)
N13–H42···O6	1.033	1.910	2.921	165.3	0.050
C17–H32···O8	1.089	2.264	3.195	142.1	0.022
C28–H41···O10	1.091	2.266	3.259	150.3	0.021
C26–H36···O7	1.090	2.286	3.317	156.9	0.020
C20–H34···O6	1.091	2.628	3.618	159.2	0.014
C31–H43···O10	1.093	2.280[a]	2.767	104.7	0.013
C31–H44···O9	1.095	2.753	3.828	167.2	0.012
C28–H41···C16	1.091	2.516[a]	2.814	94.1	0.010

[a]Intramolecular.

https://doi.org/10.1017/S0885715622000409 Published online by Cambridge University Press

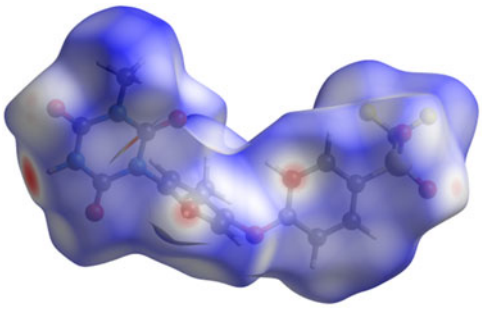

Figure 8. The Hirshfeld surface of ponazuril. Intermolecular contacts longer than the sums of the van der Waals radii are colored blue, and contacts shorter than the sums of the radii are colored red. Contacts equal to the sums of radii are white. Image generated using CrystalExplorer (Turner *et al.*, 2017).

model was included in the refinement. The texture index was 1.007(0), indicating that preferred orientation was not significant for this rotated capillary specimen.

IV. DEPOSITED DATA

The Crystallographic Information Framework (CIF) files containing the results of the Rietveld refinement (including the raw data) and the DFT geometry optimization were deposited with the ICDD. The data can be requested at pdj@icdd.com.

ACKNOWLEDGEMENTS

The use of the Advanced Photon Source at Argonne National Laboratory was supported by the U.S. Department of Energy, Office of Science, Office of Basic Energy Sciences, under Contract No. DE-AC02-06CH11357. This work was partially supported by the International Centre for Diffraction Data. We thank Lynn Ribaud and Saul Lapidus for their assistance in the data collection.

CONFLICT OF INTEREST

The authors have no conflict of interest to declare.

Altomare, A., Cuocci, C., Giacovazzo, C., Moliterni, A., Rizzi, R., Corriero, N., and Falcicchio, A. (**2013**). "EXPO2013: a kit of tools for phasing crystal structures from powder data," J. Appl. Crystallogr. **46**, 1231–1235.

Antao, S. M., Hassan, I., Wang, J., Lee, P. L., and Toby, B. H. (**2008**). "State-of-the-art high-resolution powder X-ray diffraction (HRPXRD) illustrated with Rietveld refinement of quartz, sodalite, tremolite, and meionite," Can. Mineral. **46**, 1501–1509.

Bernstein, J., Davis, R. E., Shimoni, L., and Chang, N. L. (**1995**). "Patterns in hydrogen bonding: functionality and graph set analysis in crystals," Angew. Chem. Int. Ed. Engl. **34**(15), 1555–1573.

Bravais, A. (**1866**). *Etudes Cristallographiques* (Gauthier Villars, Paris).

Bruno, I. J., Cole, J. C., Kessler, M., Luo, J., Motherwell, W. D. S., Purkis, L. H., Smith, B. R., Taylor, R., Cooper, R. I., Harris, S. E., and Orpen, A. G. (**2004**). "Retrieval of crystallographically-derived molecular geometry information," J. Chem. Inf. Sci. **44**, 2133–2144.

Crystal Impact - Dr. H. Putz & Dr. K. Brandenburg (**2022**). *Diamond - Crystal and Molecular Structure Visualization.* Kreuzherrenstr. 102, 53227 Bonn, Germany. Available at: https://www.crystalimpact.de/diamond.

Dassault Systèmes (**2021**). *Materials Studio 2021* (BIOVIA, San Diego, CA).

Donnay, J. D. H. and Harker, D. (**1937**). "A new law of crystal morphology extending the law of Bravais," Am. Mineral. **22**, 446–447.

Dovesi, R., Erba, A., Orlando, R., Zicovich-Wilson, C. M., Civalleri, B., Maschio, L., Rerat, M., Casassa, S., Baima Salustro, J., and Kirtman, B. (**2018**). "Quantum-mechanical condensed matter simulations with CRYSTAL," WIREs Comput. Mol. Sci. **8**, e1360.

Etter, M. C. (**1990**). "Encoding and decoding hydrogen-bond patterns of organic compounds," Acc. Chem. Res. **23**(4), 120–126.

Friedel, G. (**1907**). "Etudes sur la loi de Bravais," Bull. Soc. Fr. Mineral. **30**, 326–455.

Gates-Rector, S. and Blanton, T. (**2019**). "The Powder Diffraction File: a quality materials characterization database," Powd. Diffr. **39**(4), 352–360.

Gatti, C., Saunders, V. R., and Roetti, C. (**1994**). "Crystal-field effects on the topological properties of the electron-density in molecular crystals - the case of urea," J. Chem. Phys. **101**, 10686–10696.

Groom, C. R., Bruno, I. J., Lightfoot, M. P., and Ward, S. C. (**2016**). "The Cambridge Structural Database," Acta Crystallogr. Sect. B: Struct. Sci., Cryst. Eng. Mater. **72**, 171–179.

Hirshfeld, F. L. (**1977**). "Bonded-atom fragments for describing molecular charge densities," Theor. Chem. Acta **44**, 129–138.

Kaduk, J. A., Crowder, C. E., Zhong, K., Fawcett, T. G., and Suchomel, M. R. (**2014**). "Crystal structure of atomoxetine hydrochloride (Strattera), $C_{17}H_{22}NOCl$," Powd. Diffr. **29**(3), 269–273.

Kim, S., Chen, J., Cheng, T., Gindulyte, A., He, J., He, S., Li, Q., Shoemaker, B. A., Thiessen, P. A., Yu, B., Zaslavsky, L., Zhang, J., and Bolton, E. E. (**2019**). "PubChem 2019 update: improved access to chemical data," Nucleic Acids Res. **47**(D1), D1102–D1109. doi:10.1093/nar/gky1033.

Kresse, G. and Furthmüller, J. (**1996**). "Efficiency of ab-initio total energy calculations for metals and semiconductors using a plane-wave basis set," Comput. Mater. Sci. **6**, 15–50.

Lee, P. L., Shu, D., Ramanathan, M., Preissner, C., Wang, J., Beno, M. A., Von Dreele, R. B., Ribaud, L., Kurtz, C., Antao, S. M., Jiao, X., and Toby, B. H. (**2008**). "A twelve-analyzer detector system for high-resolution powder diffraction," J. Synchrotron Radiat. **15**(5), 427–432.

Li, B., Wang, Y., Feng, Y., Yuan, D., Xu, R., Jiang, C., Xiao, X., and Lu, S. (**2022**). "Design and molecular insights of drug-active metabolite base co-amorphous formulation: a case study of toltrazuril-ponazuril co-amorphous," Int. J. Pharmaceutics **615**, 121475.

Macrae, C. F., Sovago, I., Cottrell, S. J., Galek, P. T. A., McCabe, P., Pidcock, E., Platings, M., Shields, G. P., Stevens, J. S., Towler, M., and Wood, P. A. (**2020**). "*Mercury 4.0*: from visualization to design and prediction," J. Appl. Crystallogr. **53**, 226–235.

Materials Design (**2016**). *MedeA 2.20.4* (Materials Design Inc, Angel Fire, NM).

MDI (**2022**). *JADE Pro Version 8.2 (Computer Software)* (Materials Data, Livermore, CA, USA).

Peintinger, M. F., Vilela Oliveira, D., and Bredow, T. (**2013**). "Consistent Gaussian basis sets of triple-zeta valence with polarization quality for solid-state calculations," J. Comput. Chem. **34**, 451–459.

Shields, G. P., Raithby, P. R., Allen, F. H., and Motherwell, W. S. (**2000**). "The assignment and validation of metal oxidation states in the Cambridge Structural Database," Acta Crystallogr. Sect. B: Struct. Sci. **56**(3), 455–465.

Silk Scientific (**2013**). *UN-SCAN-IT 7.0* (Silk Scientific Corporation, Orem, UT).

Sykes, R. A., McCabe, P., Allen, F. H., Battle, G. M., Bruno, I. J., and Wood, P. A. (**2011**). "New software for statistical analysis of Cambridge Structural Database data," J. Appl. Crystallogr. **44**, 882–886.

Toby, B. H. and Von Dreele, R. B. (**2013**). "GSAS II: the genesis of a modern open source all purpose crystallography software package," J. Appl. Crystallogr. **46**, 544–549.

Turner, M. J., McKinnon, J. J., Wolff, S. K., Grimwood, D. J., Spackman, P. R., Jayatilaka, D., and Spackman, M. A. (**2017**). CrystalExplorer17 (University of Western Australia). Available at: http://hirshfeldsurface.net.

van de Streek, J. and Neumann, M. A. (**2014**). "Validation of molecular crystal structures from powder diffraction data with dispersion-corrected density functional theory (DFT-D)," Acta Crystallogr. Sect. B: Struct. Sci., Cryst. Eng. Mater. **70**(6), 1020–1032.

Wang, J., Toby, B. H., Lee, P. L., Ribaud, L., Antao, S. M., Kurtz, C., Ramanathan, M., Von Dreele, R. B., and Beno, M. A. (**2008**). "A dedicated powder diffraction beamline at the advanced photon source: commissioning and early operational results," Rev. Sci. Instrum. **79**, 085105.

Wavefunction, Inc. (**2020**). Spartan '18 Version 1.4.5, Wavefunction Inc., 18401 Von Karman Ave., Suite 370, Irvine, CA 92612.

Wheatley, A. M. and Kaduk, J. A. (**2019**). "Crystal structures of ammonium citrates," Powd. Diffr. **34**, 35–43.